MURPHYS-HSFS-2014 IOP Publishing
Journal of Physics: Conference Series **727** (2016) 012012 doi:10.1088/1742-6596/727/1/012012

Robust homoclinic orbits in planar systems with Preisach hysteresis operator

Alexander Pimenov
Weierstrass Institute, Mohrenstr. 39, 10117 Berlin
E-mail: alexander.pimenov@wias-berlin.de

Dmitrii Rachinskii
Department of Mathematical Sciences, The University of Texas at Dallas, TX, USA
E-mail: Dmitry.Rachinskiy@utdallas.edu

Abstract. We construct examples of robust homoclinic orbits for systems of ordinary differential equations coupled with the Preisach hysteresis operator. Existence of such orbits is demonstrated for the first time. We discuss a generic mechanism that creates robust homoclinic orbits and a method for finding them. An example of a homoclinic orbit in a population dynamics model with hysteretic response of the prey to variations of the predator is studied numerically.

1. Introduction

The theory of hysteresis operators developed in [1–3] as well as other mathematical descriptions of hysteresis (such as differential inclusions [4], differential inequalities [5] and variational descriptions of rate-independent processes [6]) allow one to analyze stability [7, 8], bifurcations [9–12] and complex dynamics [13] of systems exhibiting hysteresis. Coupled systems of differential equations and hysteresis operators have been used to model mechanical [2, 14, 15], electro-magnetic [16, 17], electro-mechanical [18, 19] and engineered systems [20–22], phase transition processes [3, 23], dynamics of fluids in porous materials [24, 25], dynamics of populations [26–28] and economic systems [29–31]; see [32] for further examples of applications. In particular, these models include ordinary differential equations coupled with the Preisach hysteresis operator that contain the time derivative of the output of the Preisach operator. Although more complex situations are possible, a generic solution of such a system can be obtained by matching solutions of several ordinary differential systems (the switching points from one to another system include the turning points of the input of the Preisach operator as well as some values stored by the dynamic memory configuration of this operator) [33–35]. While these ordinary differential systems are different, they all have the same set of equilibrium points [36].

This picture suggests a possibility of existence of robust homoclinic trajectories in the system with hysteresis operator provided that (a) the same point is a stable equilibrium of one ordinary differential system and, simultaneously, an unstable equilibrium of the other; and, (b) a trajectory of the first system converging to this equilibrium point in forward time could be

matched with a trajectory of the second system converging to the same point in backward time in such a way that the system with hysteresis would switch from the second trajectory to the first trajectory. The concatenation of the two trajectories would then form a homoclinic loop of the differential system with the hysteresis operator.

In this work, we show the existence of such homoclinic trajectories. To the best of our knowledge, homoclinic trajectories of systems with hysteresis operators have not been discussed before.

Existence of homoclinic trajectories in the systems with Preisach operator under the time derivative is closely related to the so-called *partially stable* equilibria [36], i.e. unstable equilibria, which have an open basin of attraction (in the infinite-dimensional phase space of the system). Such equilibria simultaneously attract and repel many trajectories, and they can be compared to a saddle-node singular point of an ordinary differential system, however they are robust. Systems with Preisach operator available in the literature do not demonstrate abundance of partially stable equilibria, and, moreover, it is even harder to find special kind of partially stable equilibria that would lead to the appearance of robust homoclinic orbits in such systems. We present our results in the context of mathematical ecology. Namely, we are motivated by a predator-prey system [37], where the prey switches between two modes of behaviour, safe and risky, in response to varying abundance of predator. Similar type of non-hysteretic safe-risky adaptive behaviour of the prey in response to the pressure of the predation was recently suggested as a possible mechanism leading to the so-called predator pit phenomena, where a bistability between two steady states with nonzero predator-prey densities appears [38]. When the switch between two modes of behaviour becomes hysteretic, one can observe numerically the existence of a robust homoclinic cycle [37].

We first construct a few examples of simple systems that have homoclinic orbits (Section 2). Then we give a numerical evidence of the existence of such orbits in a more complex predator-prey model with a refuge patch where we assume hysteresis in the reaction of the prey to variations of the predator abundance (Section 3). Unlike the familiar homoclinic orbits of ordinary differential systems, the homoclinic trajectories that we obtain are robust, that is they are preserved under variations of parameters and more general (sufficiently small) perturbations. Moreover, our systems typically have a continuous family of homoclinic orbits.

2. Examples of homoclinic orbits

2.1. Preisach operator

In this work we consider a coupled system of differential equations

$$\dot{u} = f(u,v) + \dot{x}h(u,v), \qquad \dot{v} = g(u,v) \tag{1}$$

and an operator equation

$$x(t) = (\mathcal{P}[\eta_0]v)(t), \tag{2}$$

where $t \geq t_0$, and $f, h, g : \mathbb{R}^2 \to C^1$.

The Preisach operator is defined by

$$(\mathcal{P}[\eta_0]v)(t) = \int_0^\infty \int_0^{\alpha_S} \mu(\alpha_R, \alpha_S)(R_{\alpha_R,\alpha_S}[\eta_0(\alpha_R,\alpha_S)]v)(t)\, d\alpha_R d\alpha_S, \tag{3}$$

where $v = v(t)$, $t \geq t_0$ is the input; the function $\eta_0 = \eta_0(\alpha_R, \alpha_S)$ which takes values 0 and 1 is the initial state function; $\mu(\alpha_R, \alpha_S)$ is an integrable density function; and R_{α_R,α_S} is the

non-ideal relay operator with thresholds α_R, α_S satisfying $\alpha_R \le \alpha_S$:

$$(R_{\alpha_R,\alpha_S}[\eta_0]v)(t) = \begin{cases} 0 & \text{if} \quad v(\tau) \le \alpha_R \text{ for some } \tau \in [t_0, t] \\ & \quad \text{and } v(s) < \alpha_S \text{ for all } s \in [\tau, t]; \\ 1 & \text{if} \quad v(\tau) \ge \alpha_S \text{ for some } \tau \in [t_0, t] \\ & \quad \text{and } v(s) > \alpha_R \text{ for all } s \in [\tau, t]; \\ \eta_0(\alpha_R, \alpha_S) & \text{if} \quad \alpha_R < v(\tau) < \alpha_S \text{ for all } \tau \in [t_0, t]. \end{cases} \tag{4}$$

We represent states (4) of the relays graphically on the half-plane $\{(\alpha_R, \alpha_S)\colon\ \alpha_R \le \alpha_S\}$, which is divided into two parts by a staircase polyline $\Omega = \Omega(t)$ with the relays in state 1 below (to the left) of this line and in state 0 above (to the right) of this line, see Fig. 1 (left). At any moment $t \ge t_0$ the right end point of $\Omega(t)$ is the point $\alpha_R = \alpha_S = v(t)$ [1]. For simplicity, the measure $\mu(\alpha_R, \alpha_S)$ is often assumed to have triangular support $\alpha_m \le \alpha_R \le \alpha_S \le \alpha_M$, hence we are interested only in the representation of the states of the relays inside this triangle.

The staircase polyline $\Omega(t)$ changes over time in accordance with formula (4) in response to variations of continuous non-negative input $v(t)$. We illustrate the evolution of $\Omega(t)$ with time $t \ge t_0$ using the following example with $\alpha_m = 0$. Let $\Omega(t_0)$ be the horizontal segment $\alpha_S = v(t_0)$, $0 \le \alpha_R \le v(t_0)$ (see Fig. 1, right). If $v(t)$ monotonically decreases on an interval $t \in [t_0, t_1]$, then $\Omega(t)$ acquires the vertical link $\alpha_R = v(t)$, $v(t) \le \alpha_S \le v(t_0)$ as shown in Fig. 2, left. Now, suppose that the input monotonically increases for $t \in [t_1, t_3]$. Then $\Omega(t)$ acquires a new horizontal link $\alpha_S = v(t)$, $v(t_1) \le \alpha_R \le v(t) < v(t_0)$ (see Fig. 2, right). If the input reaches its initial value $v(t_0)$ at some moment t_2^*, then $\Omega(t_2^*)$ coincides with the initial horizontal segment $\Omega(t_0)$ (Fig. 1, right). For $t \in [t_2^*, t_3]$ the input further increases and $\Omega(t)$ remains horizontal until $v(t)$ reaches a maximum $v(t_3)$ (Fig. 3, left). If $v(t)$ decreases after the moment t_3, then $\Omega(t)$ acquires a vertical link, see Fig. 3, right. This example demonstrates how the staircase polyline $\Omega(t)$ can acquire and loose multiple vertical and horizontal links in response to variations of the input $v(t)$; for more details see [13]. Below $\Omega(t)$ is referred to as the polyline of the state $\eta(t)$ of the Preisach operator or, simply, the state.

In equations (1), (2), the derivative of the output of the Preisach operator is used. For the evaluation of this derivative, the most right link $\Omega_e = \Omega_e(t)$ which is attached to the right end point $\alpha_R = \alpha_S = v(t)$ of the staircase polyline $\Omega(t)$ is important, see Fig. 4, left (if Ω has infinitely many links, then $\Omega_e = \emptyset$). Denote by $(v_m, v), (v, v_M)$ the end points of the segment Ω_e, where $v_m = v$ if Ω_e is a vertical segment and $v_M = v$ if Ω_e is horizontal. If $v = v(t)$ increases, then the time derivative of the output of the Preisach operator satisfies [33]

$$\frac{d(\mathcal{P}[\eta_0]v)}{dt} = \dot{v} H(v, v_m) \quad \text{with} \quad H(v, v_m) = \int_{v_m}^{v} \mu(\alpha_R, v)\, d\alpha_R. \tag{5}$$

If v decreases, then

$$\frac{d(\mathcal{P}[\eta_0]v)}{dt} = \dot{v} V(v, v_M) \quad \text{with} \quad V(v, v_M) = \int_{v}^{v_M} \mu(v, \alpha_S)\, d\alpha_S. \tag{6}$$

2.2. Homoclinic solutions

Equilibria of the system (1), (2) can be obtained by setting all the derivatives including the derivative $\dot{x}$ of the Preisach operator to zero.

Definition 1. *We call a solution* (u^*, v^*) *of the equations* $f(u^*, v^*) = 0$, $g(u^*, v^*) = 0$ *an equilibrium of the system* (1), (2).

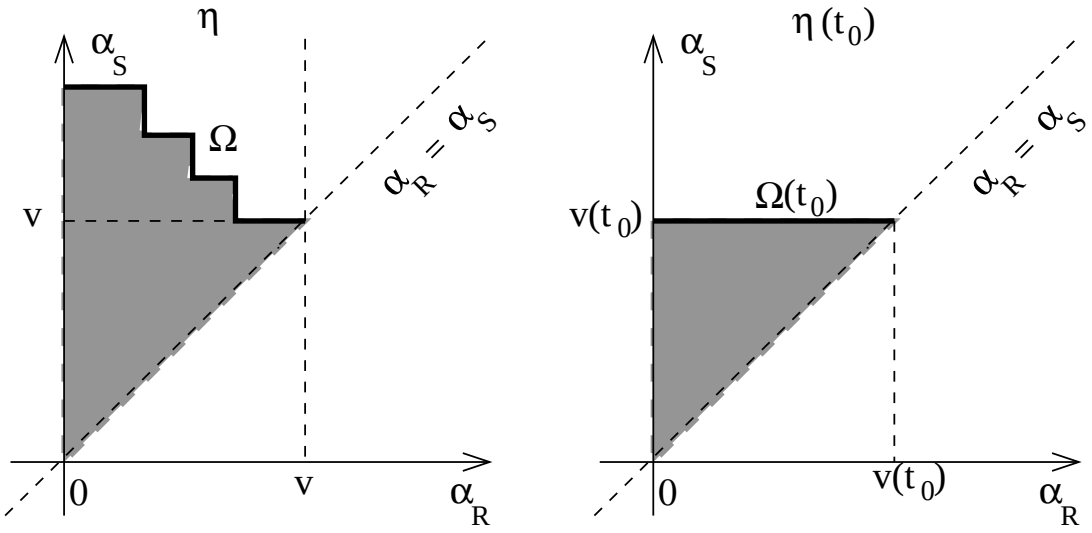

Figure 1. The domain $\{(\alpha_R, \alpha_S)\colon\ \alpha_m \le \alpha_R \le \alpha_S\}$ with $\alpha_m = 0$ is divided into two parts by a staircase polyline $\Omega = \Omega(t)$ with the relays in state 1 below (to the left) of this line (grey colour) and in state 0 above (to the right) of this line (white colour). Here all relays with $\alpha_S \le v$ are in the state 1, all relays with $\alpha_R \ge v$ are in the state 0, and the state of other relays is defined by the polyline Ω. In the right figure $\Omega(t_0)$ is the horizontal segment $\alpha_S = v(t_0)$, $0 \le \alpha_R \le v(t_0)$.

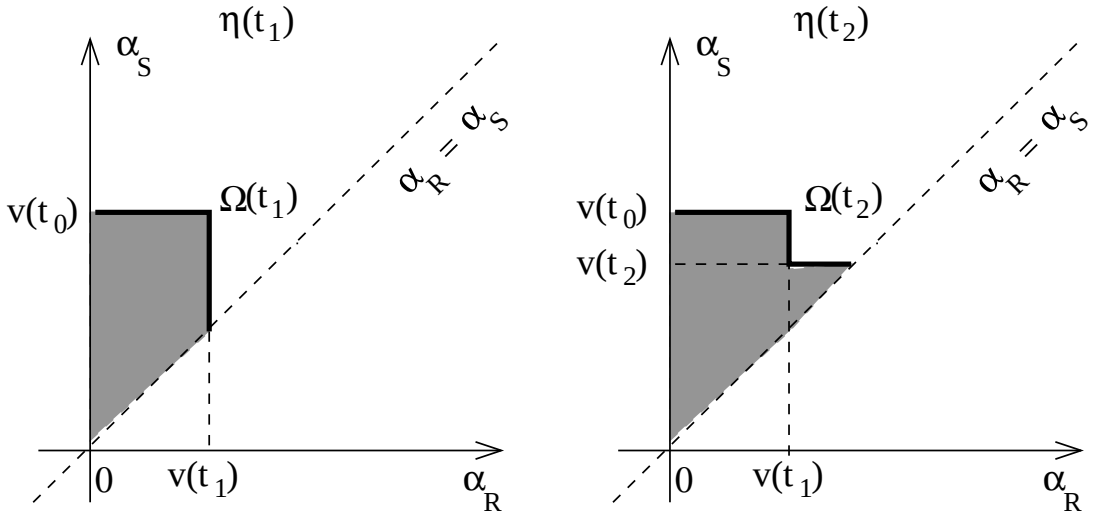

Figure 2. Evolution of the staircase polyline $\Omega = \Omega(t)$ from the initial state $\Omega(t_0)$ shown in Fig. 1 (right) in response to an input $v(t)$. For $t_0 < t \le t_1$ the input $v(t)$ monotonically decreases, and the line Ω consists of two segments (left panel, $t = t_1$): the vertical link $\alpha_R = v(t)$, $v(t) \le \alpha_S \le v(t_0)$ connects to the horizontal link, which is a part of the segment $\Omega(t_0)$ shown in Fig. 1 (right). For $t_1 < t \le t_2$ the input $v(t)$ monotonically increases, where $v(t_1) < v(t_2) < v(t_0)$, and the state Ω has three links as shown on the right panel for the moment $t = t_2$. The leftmost horizontal link and the vertical link of the line $\Omega(t_2)$ are parts of the staircase $\Omega(t_1)$ presented on the left panel, and the rightmost horizontal link is $\alpha_S = v(t_2)$, $v(t_1) \le \alpha_R \le v(t_2)$.

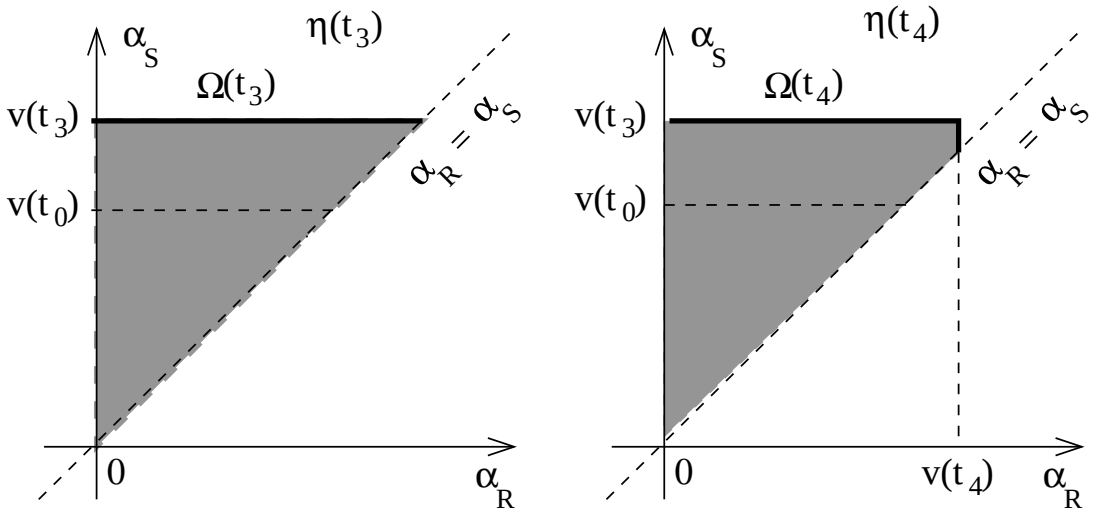

Figure 3. Evolution of $\Omega(t)$ from the state $\Omega(t_2)$ shown in Fig. 2 (right). For $t_2 \le t < t_3$ the input $v(t)$ monotonically increases and, at the moment $t_2^* \in [t_2, t_3)$, reaches the value $v(t_2^*) = v(t_0)$. The state $\Omega(t_2^*)$ becomes the horizontal segment (which coincides with $\Omega(t_0)$) and remains the horizontal segment $\alpha_S = v(t)$, $0 \le \alpha_R \le v(t)$ for all $t_2^* \le t \le t_3$ (that is, as long as the input increases), as shown on the left panel. After the moment t_3 the input $v(t)$ decreases again, and the state $\Omega(t_4)$ presented on the right panel for a moment $t_4 > t_3$ is similar to the staircase in Fig. 2 (left).

Every equilibrium defines stationary solutions $\{u(t), v(t), \eta(t)\} \equiv \{u^*, v^*, \eta_0\}$ of system (1), (2).

Assume that system (1), (2) has an equilibrium. Without loss of generality, assume that $u^* = v^* = 0$. Since the output of the Preisach operator (2) is defined on a semiaxis $t \ge t_0$, we use the following definition of a solution to system (1), (2) on the whole axis $t \in \mathbb{R}$.

Definition 2. *A triplet $\{u(t), v(t), \eta(t)\}$ is a solution of* (1), (2) *if for each t_0 this triplet is a solution of* (1), (2) *with the initial values $u_0 = u(t_0), v_0 = v(t_0), \eta_0 = \eta(t_0)$ on the semiaxis $t \ge t_0$.*

Definition 3. *We call a solution* $\{u(t), v(t), \eta(t)\}$ homoclinic *if $u(t) \to 0, v(t) \to 0$ for $t \to \pm\infty$, and either $u(t) \ne 0$ or $v(t) \ne 0$ for all $t \in \mathbb{R}$.*

In this work, we focus on the piecewise monotone homoclinic solutions $\{u(t), v(t), \eta(t)\}$ with *monotone tails.*

Assumption 1. *There exist $t_1, t_2 \in \mathbb{R}$ such that $t_1 \le t_2$, and the component v of the homoclinic solution $\{u(t), v(t), \eta(t)\}$ is monotone for $t \le t_1$ and for $t \ge t_2$.*

For such trajectories we can define the limit of the state of the Preisach operator at $t \to \pm\infty$. We will write $\eta(t) \to \eta^*$ as $t \to -\infty$ (or, as $t \to \infty$) if the polyline $\Omega(t)$ of $\eta(t)$ converges to the polyline Ω^* of η^* (as a set on the plane (α_R, α_S)).

2.3. Existence of robust homoclinic orbits

To demonstrate rigorously the possibility of existence of homoclinic orbits, we consider the following example of system (1):

$$\dot u = au + bv - \kappa(\dot x - |cu + dv|v), \qquad \dot v = cu + dv \tag{7}$$

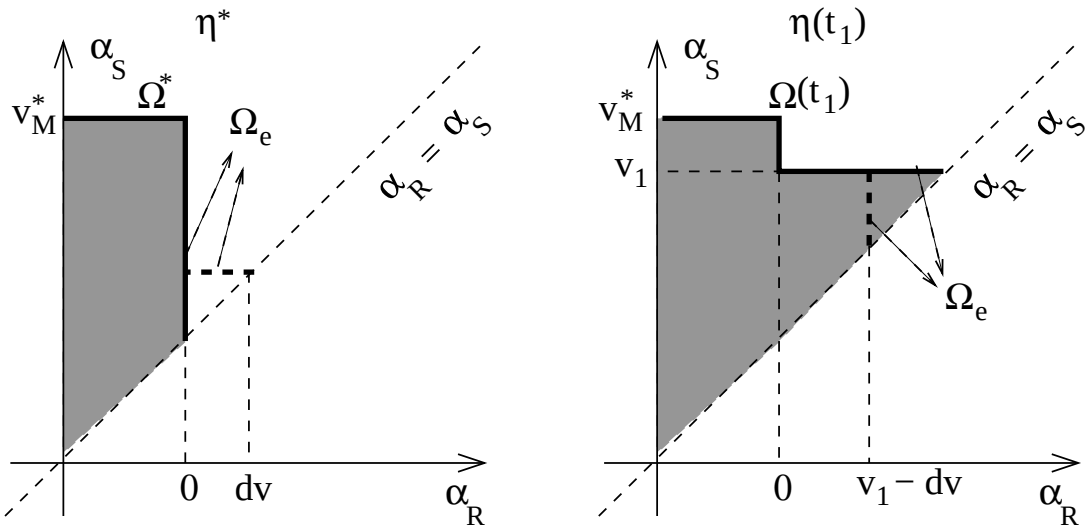

Figure 4. Evolution of the polyline $\Omega(t)$ for an input $v(t)$ that has one maximum point $v(t_1) = v_1$; $\Omega_e(t)$ is the segment of this staircase polyline with the end point $\alpha_R = \alpha_S = v(t)$ on the bisector. The limit state Ω^* (solid line on the left panel) in this example consists of a horizontal segment and the vertical segment Ω_e^*. During the time interval $(-\infty, t_1]$ when the input $v(t)$ increases, $\Omega(t)$ has three segments, the segment $\Omega_e(t)$ is horizontal (thick dashed line). The right panel shows the state $\Omega(t_1)$ (solid line) at the moment when the input achieves its maximum $v(t_1) = v_1$. After this moment, the input decreases, $\Omega(t)$ consists of four segments, the segment $\Omega_e(t)$ is vertical (thick dashed line).

and assume that the density function of the Preisach operator (2) is uniform, $\mu(\alpha_R, \alpha_S) \equiv 1$. This system has an equilibrium at zero, $u = v = 0$.

First, we prove the existence of a simple homoclinic orbit with the limit state η^* shown in Fig. 4 (left) such that the polyline Ω^* has a sufficiently long vertical segment $\Omega_e^* = \{(\alpha_R, \alpha_S) : \alpha_R = 0,\ \alpha_S \in [0, v_M]\}$. We aim to construct a homoclinic trajectory with a component $v(t)$ that increases for $t < t_1$, decreases for $t > t_1$ and has one maximum point $v(t_1)$ (cf. Assumption 1), see Fig. 5.

Proposition 1. *Assume that*

$$\Delta = ad - bc > 0,\ \tau = a + d > 0,\ D = \tau^2 - 4\Delta > 0, \tag{8}$$

$\kappa c > 0$, *and the segment* Ω_e^* *of the polyline* Ω^* *of the state* η^* *is vertical with the end points* $(\alpha_R, \alpha_S) = (0, 0)$ *and* $(\alpha_R, \alpha_S) = (0, v_M^*)$, *where* $v_M^* > \frac{a+d+2\sqrt{\Delta}}{c\kappa} =: v_{1m}$. *Then, for each* $v_1 \in (v_{1m}, v_M^*]$ *there is a homoclinic solution* $\{u(t), v(t), \eta(t)\}$ *such that* $v(t_1) = v_1$ *is a single extremum point of the component* $v(t)$, *which is a point of maximum. That is, system* (2), (7) *has infinitely many robust homoclinic trajectories satisfying* $\eta(t) \to \eta^*$ *as* $t \to \pm\infty$.

Robustness means that the continual set of homoclinic trajectories persists under perturbations of system parameters.

Proof. A homoclinic solution of system (2), (7) described in this proposition satisfies relation (5) with $v_m = 0$ for $t < t_1$ and relationship (6) with $v_M = v_1$ for $t > t_1$. Hence, for such a solution, $\dot{x} = v\dot{v}$ for $t < t_1$ and $\dot{x} = (v_1 - v)\dot{v}$ for $t > t_1$ (where we use the relationship $\mu(\alpha_R, \alpha_S) \equiv 1$ when calculating $H(v, 0)$ and $V(v, v_1)$). Substituting these expressions for $\dot{x}$ in (7), we see that

the homoclinic solution satisfies the linear differential system

$$\dot{u} = au + bv, \qquad \dot{v} = cu + dv \tag{9}$$

on the semiaxis $t < t_1$; and, the linear differential system

$$\dot{u} = (a - \kappa v_1 c)u + (b - \kappa v_1 d)v, \qquad \dot{v} = cu + dv \tag{10}$$

on the semiaxis $t > t_1$; the point $(u(t_1), v(t_1)) = (u_1, v_1)$ lies on the nullcline $\dot{v} = cu + dv = 0$ of these systems, as v_1 is the maximum value of the v-component. Furthermore, to prove the proposition it suffices to show that for every $v_1 \in (v_{1m}, v_M^*] \subset (0, v_M^*]$:

(a) The solution of system (9) with the initial conditions $u(t_1) = -dv_1/c$, $v(t_1) = v_1$ satisfies $\dot{v} > 0$ for all $t < t_1$ and $v \to 0$ as $t \to -\infty$;

(b) The solution of system (10) with the same initial conditions $u(t_1) = -dv_1/c$, $v(t_1) = v_1$ satisfies $\dot{v} < 0$ for all $t > t_1$ and $v \to 0$ as $t \to \infty$.

Here (a) follows from conditions (8), which ensure that the zero equilibrium of system (9) is a proper unstable node; (b) follows from the relationship $v_1 > v_{1m}$, which implies that the zero equilibrium of system (9) is a proper asymptotically stable node. □

The case $\kappa c < 0$ can be considered similarly. In this case, the following analog of Proposition 1 is valid.

Proposition 2. *Assume that conditions* (8) *and* $\kappa c < 0$ *hold and the segment* Ω_e^* *of the polyline* Ω^* *of the state* η^* *is horizontal with the end points* $(\alpha_R, \alpha_S) = (0, 0)$ *and* $(\alpha_R, \alpha_S) = (v_m^*, 0)$ *with* $v_m^* < -v_{1m}$*, where* v_{1m} *is defined in Proposition 1. Then, for each* $v_1 \in [v_m^*, -v_{1m})$ *there is a homoclinic trajectory with* $\min_{t\in\mathbb{R}} v(t) = v_1$*. That is, system* (2), (7) *has infinitely many robust homoclinic trajectories satisfying* $\eta(t) \to \eta^*$ *as* $t \to \pm\infty$ *such that the* v*-component of the trajectory has a single extremum point, which is a point of minimum.*

As the last example of this section, we consider homoclinic trajectories which have more complex limit states η^* at $t \to -\infty$, see in Fig. 6, and more than two monotonicity intervals of the v-component, see Fig. 7.

Proposition 3. *Assume that conditions* (8) *hold,* $\kappa c > 0$ *and the polyline* Ω^* *of state* η^* *includes three links connecting the corner points* $(0, 0)$, $(0, v_M^*)$, (v_m^*, v_M^*), (v_m^*, v_{M2}^*)*, where* $0 < v_M^* < \frac{a+d-2\sqrt{\Delta}}{c\kappa} =: v_{1M}$, $v_{M2}^* > \frac{a+d+2\sqrt{\Delta}}{c\kappa} =: v_{1m}$*, and* $v_m^* < -v_{1m}$*. Then system* (2), (7) *has a robust homoclinic trajectory with the limit state* $\eta(t) \to \eta^*$ *as* $t \to -\infty$*. The* v*-component of this trajectory has a single maximum point and a single minimum point with* $\max_{t\in\mathbb{R}} v(t) = v_M^*$ *and* $\min_{t\in\mathbb{R}} v(t) < v_m^*$*.*

We note that the homoclinic solution described in this proposition has different limit states at $t \to \pm\infty$, that is $\lim_{t\to\infty} \eta(t) \neq \lim_{t\to-\infty} \eta(t) = \eta^*$. As a matter of fact, there are again infinitely many homoclinic trajectories with the maximum value $v_1 = \max_{t\in\mathbb{R}} v(t)$ of the v-component ranging over the interval $v_1 \in (0, v_M^*]$. We consider one of these trajectories as an example.

Proof. The proof is similar to that of Proposition 1. Here, it suffices to show that:

(a) The solution of system (9) with the initial point $u(t_1) = -dv_M^*/c$, $v(t_1) = v_M^*$ on the nullcline $\dot{v} = cu + dv = 0$ satisfies $\dot{v} > 0$ for all $t < t_1$ and $v \to 0$ as $t \to -\infty$;

(b) The solution of system (10) with $v_1 = v_M^*$ starting from the initial point $u(t_1) = -dv_M^*/c$, $v(t_1) = v_M^*$ satisfies $\dot{v} < 0$ on an interval $t \in (t_1, t_2]$ where the end point $(u(t_2), v(t_2)) =: (u_m, v_m)$ satisfies $v(t_2) = v_m^*$.

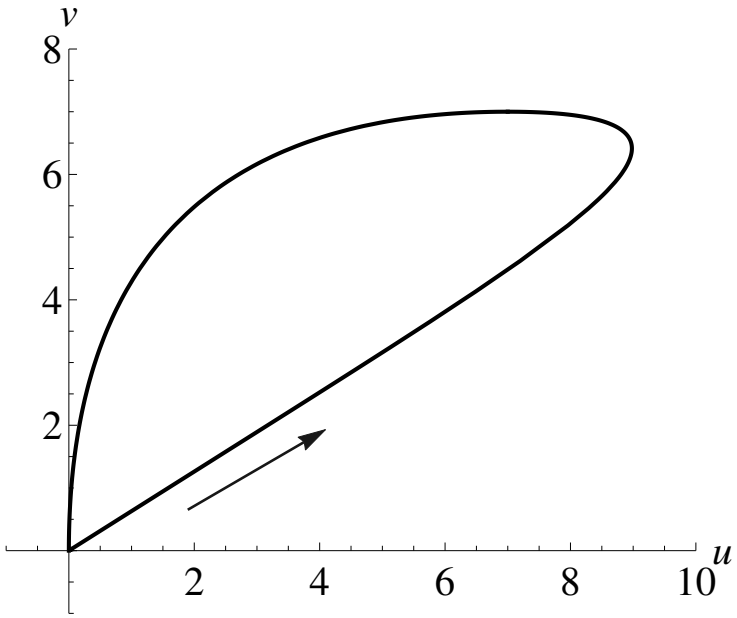

Figure 5. A homoclinic orbit of system (2), (7) satisfying the assumptions of Proposition 1 for $\kappa = 1$, $a = 5$, $b = -7$, $c = 1$, $d = -1$, $v_M^* \geq 7$. The orbit is located in the positive quadrant; the arrow shows the direction of motion; zero is the equilibrium. The maximum of the v-component is achieved at the point $u = v = 7$ of the nullcline $\dot{v} = u - v = 0$. Fig. 4 illustrates the evolution of the state $\eta(t)$ of the Preisach operator for this orbit. The solid line $\Omega = \Omega^*$ on the left panel of Fig. 4 is the polyline of the limit state η^* defined by $\eta(t) \to \eta^*$ as $t \to \pm\infty$.

(c) The solution of system (10) with $v_1 = v_{M2}^*$ starting from the initial point $(u(t_2), v(t_2)) =: (u_m, v_m^*)$ satisfies $\dot{v} < 0$ on an interval $t \in [t_2, t_3)$ where the end point $(u(t_3), v(t_3)) =: (-dv_{min}/c, v_{min})$ lies on the nullcline $\dot{v} = cu + dv = 0$.

(d) The solution of the equation

$$\dot{u} = (a + \kappa v_3 c)u + (b + \kappa v_3 d)v, \qquad \dot{v} = cu + dv \tag{11}$$

with $v_3 = v_{min}$ starting from the initial point $(u(t_3), v(t_3)) = (-dv_{min}/c, v_{min})$ on the nullcline $\dot{v} = cu + dv = 0$ satisfies $\dot{v} > 0$ for all $t > t_3$ and $v \to 0$ as $t \to \infty$.

Statement (a) follows from assumptions (8), which ensure that the zero equilibrium is a proper unstable node of system (9).

The vector fields $(\dot{u}, \dot{v})$ of systems (9) and (10) coincide on the nullcline $\dot{v} = 0$. As $\dot{v} > 0$ for $t < t_1$ for the solution of (9) with the initial condition $(u(t_1), v(t_1)) = (-dv_M^*/c, v_M^*)$ on the nullcline, it follows that the solution of (10) starting from the same initial condition satisfies $\dot{v} < 0$ for sufficiently small $t - t_1 > 0$. This solution of (10) remains in the half plane $\dot{v} = cu + dv < 0$ for all $t > t_1$ and satisfies $v \to -\infty$ as $t \to \infty$, because the assumption $v_M^* < v_{1M}$ ensures that the zero equilibrium is a proper unstable node of system (10) with $v_1 = v_M^*$. As $v_M^* > 0 > v_m^*$, this solution will eventually hit the line $v = v_m^*$ at some moment t_2 at a point (u_m, v_m^*). This proves (b).

The assumption $v_{M2}^* > v_{1m}$ implies that the zero equilibrium of system (10) with $v_1 = v_{M2}^*$ is a proper asymptotically stable node. As $v_m^* < 0$ and the point (u_m, v_m^*) lies in the half plane $\dot{v} = cu + dv < 0$, it follows that the solution of this system starting at (u_m, v_m^*) will hit the nullcline $\dot{v} = cu + dv = 0$ at some point $(-dv_{min}/c, v_{min})$, that is (c) holds.

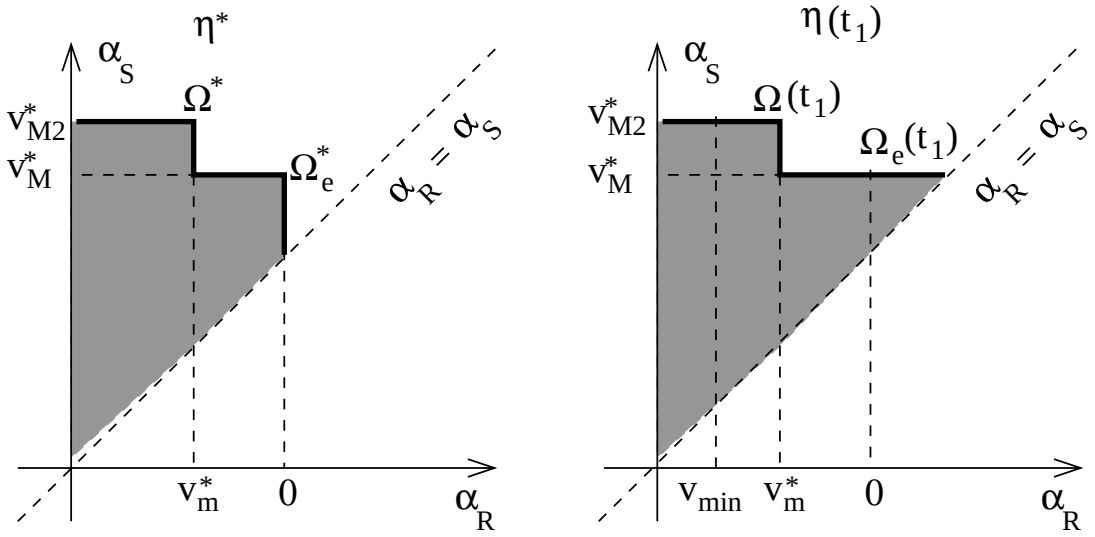

Figure 6. Evolution of the staircase polyline $\Omega(t)$ for the homoclinic trajectory described in Proposition 3. The segment $\Omega_e(t)$ of this staircase line is the link with the end point $\alpha_R = \alpha_S = v(t)$ on the bisector. The left panel shows the limit state of the homoclinic orbit at $t \to -\infty$. The right panel shows the state $\Omega(t_1)$ (solid line) at the moment when the v-component achieves its maximum value $v(t_1) = v^*_M$. After this moment, $v(t)$ decreases until it reaches its minimum value $v(t_3) = v_{min}$, then it increases and tends to zero. The polyline $\Omega(t)$ has only two links between the moment $t_2 \in (t_1, t_3)$ when the input $v(t)$ reaches the value $v(t_2) = v^*_m$ and the moment when it reaches its minimum $v(t_3) = v_{min}$.

Finally, (d) follows from the relationships $v_{min} < v^*_m < -v_{1m} < 0$, which ensure that the zero equilibrium is a proper asymptotically stable node of system (11) with $v_3 = v_{min}$. □

3. Numerical examples

3.1. Population dynamics model

In this section, we give a numerical evidence of the existence of homoclinic trajectories in a predator-prey type model [37], which has nontrivial dynamical properties such as multiple stable equilibria:

$$\dot{u} = a(u) - f(u)g(v) - h(t)u, \tag{12}$$

$$\dot{v} = \sigma f(u)g(v) - c(v), \tag{13}$$

where u is the number of prey; v is the number of predator; the term

$$a(u) = \rho u - \lambda u^2$$

describes the logistic growth of the prey with the birth rate ρ and the competition rate λ;

$$f(u) = \frac{\omega u}{\phi + u}$$

is the Holling type II functional response;

$$g(v) = \frac{v}{1 + \beta v}$$

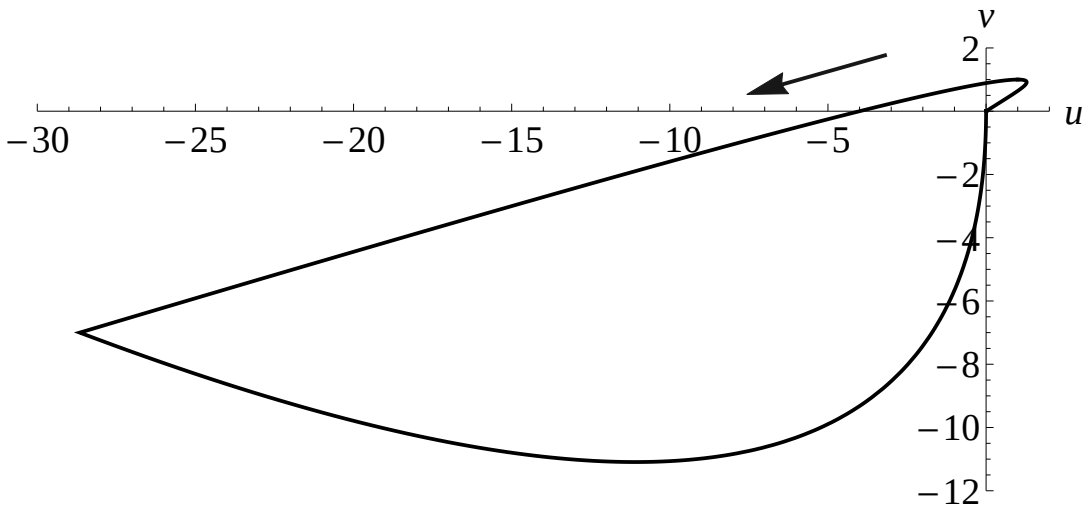

Figure 7. Homoclinic orbit of system (2), (7) satisfying the conditions of Proposition 3. The orbit converges to the zero equilibrium; the arrow shows the direction of motion. The parameters are $\kappa = 1$, $a = 5$, $b = -7$, $c = 1$, $d = -1$, $v_M^* = 1$, $v_m^* = -7$ and $v_{M2}^* = 7$. The v-component has its maximum at the point $(u(t_1), v(t_1)) = (1, 1)$ of the nullcline $\dot{v} = u - v = 0$. The trajectory makes a corner at the point $(u(t_2), v(t_2)) = (-7, -23 - 4\sqrt{2})$ of the line $v = v_m^*$ at the moment $t_2 = t_1 + \log(1 + 2\sqrt{2})$. The v-component achieves its minimum $v_{min} = -(697 + 64\sqrt{2})/71$ at the point $(u(t_3), v(t_3)) = (v_{min}, v_{min})$ of the nullcline $u - v = 0$ at the moment $t_3 = t_2 + 2\,\mathrm{artanh}(10 + \sqrt{2})/49$.

is the predator interference; σ is the efficiency of conversion of food to growth; and, the term

$$c(v) = \gamma v$$

describes death of the predator with the death rate γ (all the parameters are positive). The term $h(t)$ describes the flow of the prey to some refuge patch from which it never returns. System (12)-(13) is analagous to the two-patch predator-prey system proposed in [37], where the safe patch is completely separated from the environment; alternatively, the term $h(t)$ can be considered as an additional predator-induced death rate.

We consider the flow rate in response to the change of predator abundance in the following form:

$$h(t) = \left(k_0 + k\frac{d}{dt}(\mathcal{P}[\eta_0]v)(t) - 2k^\dagger|\dot{v}|(v - v^\dagger) \right)^+, \tag{14}$$

where we ensure that the flow satisfies $h(t) \geq 0$ using the function $x^+ = \max\{x, 0\}$, and $\dot{v}$ can be replaced with the right hand side of equation (13). The main ingredients here are the constant flow rate k_0 and the hysteretic reaction of the prey to variations of the predator abundance, $k\frac{d}{dt}(\mathcal{P}[\eta_0]v)(t)$, where hysteresis appears due to a delay of the response of the prey to a change of the trend in predator dynamics (i.e., the change of the sign of $\dot{v}$). A specific choice of the model for this hysteretic response in the form of the Preisach operator is related to a number of phenomenological assumptions. Namely, the environment is divided into many small interconnected patches, and it assumed that the change of the rate of flow of the prey to the refuge from any given patch is delayed until the abundance of the predator drops/increases from its extremum value by a certain positive amount, which is specific to the patch. More detailed derivation of the model is presented in [37]. We assume that the measure $\mu(\alpha_R, \alpha_S)$ of

the Preisach operator $\mathcal{P}[\eta_0]$ is zero outside the triangle $0 \le \alpha_R \le \alpha_S \le 1$, and $\mu(\alpha_R, \alpha_S) = 2$ inside the triangle.

The additional term $2k^\dagger|\dot{v}|(v - v^\dagger)$ in (14) strengthens the reaction of the prey to the change of the predator abundance if v is below the threshold $v^\dagger$, and weakens this reaction if v is above the threshold. In other words, the prey is attentive to the change of the predator numbers if the predator is not abundant and its attention to the predator becomes saturated for $v \gg v^\dagger$. This artificial term is similar to the term we introduced in (7) and, indeed, allows us to demonstrate numerically dynamics of (12)-(14), which are similar to dynamics of equations (2), (7). We will consider the system with ($k^\dagger > 0$) and without ($k^\dagger = 0$) this term.

In the case of increasing v, substituting formula (5) in equations (14), we obtain the following expression for the rate of flow to the refuge:

$$h(t) = \Big(k_0 + \dot{v}(kH(v, v_m) - 2k^\dagger(v - v^\dagger))\Big)^+, \tag{15}$$

where $\dot{v}$ can be replaced with the right hand side of equation (13). Similarly, when v decreases,

$$h(t) = \Big(k_0 + \dot{v}(kV(v, v_M) + 2k^\dagger(v - v^\dagger))\Big)^+. \tag{16}$$

Equilibria of system (12)-(14) can be found from the algebraic system, which is obtained by setting the derivatives of all the variables, including $d/dt(\mathcal{P}[\eta_0]v)$, to zero in (12)-(14).

Numerical examples of homoclinic orbits of system (12)-(14) presented in the next section were obtained by an algorithm, which is similar to the method used in the previous section.

3.2. Numerical results

We set $\rho = 1.35$, $\phi = 0.1$, $\beta = 1.2$, $\gamma = 0.5$, $\omega = 2$, $k_0 = 0.01$, $\lambda = 0.01$ to ensure that system (12)-(14) has three positive equilibrium points

$$(u^*, v^*) = (0.183649, 0.245752), \tag{17}$$

$$(u^\dagger, v^\dagger) = (0.340215, 0.45473), \tag{18}$$

$$(u^\ddagger, v^\ddagger) = (133.376, 0.832085). \tag{19}$$

If $k = k^\dagger = 0$ (the rate to the refuge (14) is constant, there is no hysteresis), then these equilibrium points of the ordinary differential system (12)-(14) have the eigenvalues $(0.136, 0.614)$, $(-0.089, 0.942)$, and $(-1.33, -0.25)$, respectively. That is, the first equilibrium is an unstable node, the second equilibrium is a saddle and the third equilibrium is a stable node.

When the hysteresis term is present ($k > 0$), we give a numerical evidence that equilibrium (17) can have a homoclinic orbit attached to it. We consider a constant density function of the Preisach operator (3),

$$\mu(\alpha_R, \alpha_S) = 2,$$

in the triangle $0 \le \alpha_R \le \alpha_S \le 1$ and set $\mu = 0$ outside this triangle. The integral of μ over the whole half plane $\alpha_S \ge \alpha_R$ is normalized to 1.

As the limit state of the Preisach operator, $\lim_{t\to-\infty} \eta(t) = \eta^*$, we choose the polyline $\Omega(t_0)$ which has two links: a vertical link $\Omega_e(t_0) = \{(\alpha_R, \alpha_S) : \alpha_R = v^*,\ v^* \le \alpha_S \le v_M^*\}$ and a horizontal link $\{(\alpha_R, \alpha_S) : 0 \le \alpha_R \le v^*,\ \alpha_S = v_M^*\}$, where v^* is the second component of equilibrium (17) (see Fig. 4, left, where the origin is shifted to the point $\alpha_R = \alpha_S = v^*$).

First, we consider system (12)-(14) with $k = k^\dagger = 8000$ and $v^\dagger = 0.246 > v^*$. The parameter v_M^* of the limit state for this example is set to $v_M^* = 1$. We solve the ordinary differential system (12), (13), (15) with $v_m = v^*$ numerically backward in time using as the

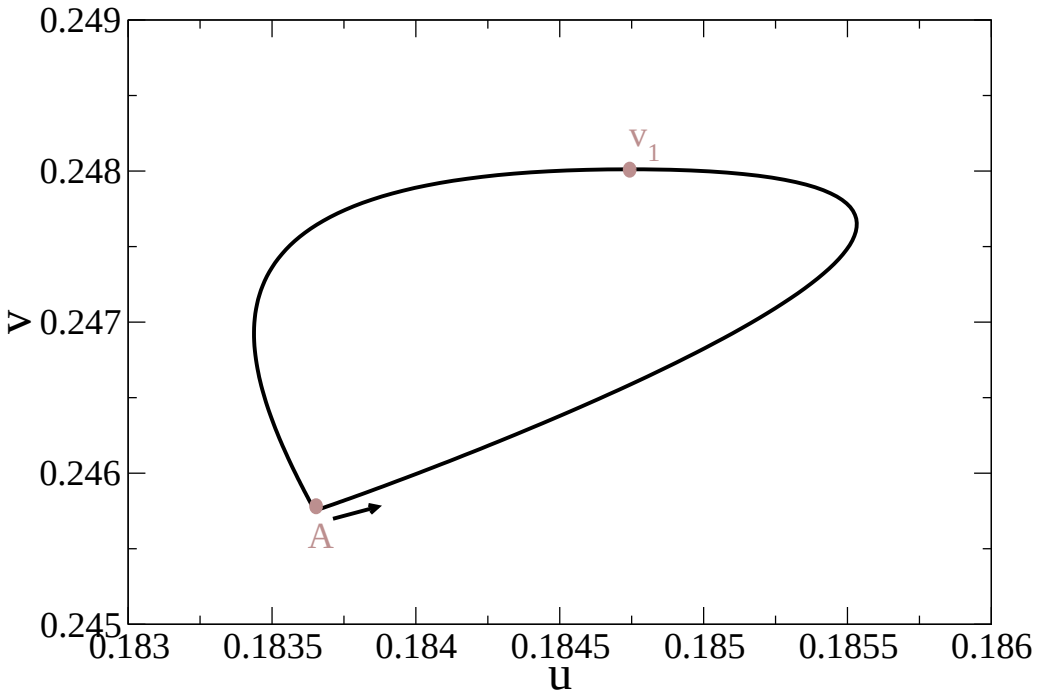

Figure 8. Homoclinic loop of system (12)-(14) with $k = k^\dagger = 8000$, $v^\dagger = 0.246$ and equilibrium (17) at the point A.

initial value a point $(u_1, v_1) = (v(t_0), v(t_0)) \approx (0.248, 0.185)$ on the nullcline $\dot{v} = 0$. The eigenvalues of the equilibrium (17) for this system are $(0.136, 0.614)$. We check that $\dot{v} > 0$ for $t < t_0$, and the solution $(u(t), v(t))$ approaches (u^*, v^*) as t decreases (see Fig. 8): $(v(t_0 - 30), u(t_0 - 30)) \approx (v^* + 3.55 \times 10^{-6}, u^* + 5.61 \times 10^{-5})$. Then we solve system (12), (13), (16) with $v_M = v_1$ numerically forward in time for $t \geq t_0$ starting from the same initial point (u_1, v_1). We observe that the solution $(u(t), v(t))$ approaches the equilibrium (u^*, v^*) and $\dot{v} < 0$ for $t > t_0$. The eigenvalues of the equilibrium (17) for this ordinary differential system are $(-5.73072, -0.0146083)$.

Next, we construct a homoclinic trajectory similar to the one shown on Fig. 7 for system (12)-(14) with $k^\dagger = 0$, $k = 700$. The parameter of the limit state is set to $v_M^* = v_1 = 0.2596$. As in the previous example, we solve system (12)-(13), (15) with $v_m = v^*$ numerically backward in time starting from the point (u_1, v_1) on the nullcline $\dot{v} = 0$ with $v(t_0) = v_1$, see Fig. 9. This solution satisfies $\dot{v} > 0$ for $t < t_0$. Then, we solve system (12)-(13), (16) with $v_M = v_1$ for $t > t_0$ starting from the same point (u_1, v_1). We observe that $v(t)$ decreases, while the trajectory spirals around the equilibrium (17) for $t_0 < t < t_{2a}$, where $t_{2a} \approx t_0 + 1.612$, because (17) is a stable focus for this ordinary differential system. However, for $t = t_{2a}$, $v(t_{2a}) \approx 0.25741$ the flow $h(t)$ in (12) becomes 0; at this point, the term $k\dot{v}V(v, v_1)$ is negative, and $|\dot{v}|$ becomes large enough to compensate for the term $k_0 > 0$ in relation (16). We observe that $k\dot{v}V(v, v_1) + k_0 < 0$ and $h(t) \equiv 0$ for $t_{2a} < t < t_{2b}$, where $t_{2b} \approx t_0 + 11.043$, $v(t_{2b}) \approx 0.0384$, and $k\dot{v}V(v, v_1) + k_0 = 0$ at $t = t_{2b}$. After this moment, $h(t)$ becomes positive again. Shortly after this point, the v-component of the solution reaches its (global) minimum $v(t_3) = v_3 \approx 0.0384$ at $t_3 \approx 11.046$ as the solution arrives at the nullcline $\dot{v} = 0$. From the nullcline, we continue the trajectory for $t > t_3$ as the solution of ordinary differential system (12)-(13), (15) with $v_m = v_3$. For this system, the equilibrium (17) has the eigenvalues $(-11.8176, -0.00708397)$ and the trajectory is attracted to the equilibrium. The component $v(t)$ increases and the term $h(t)$ remains positive

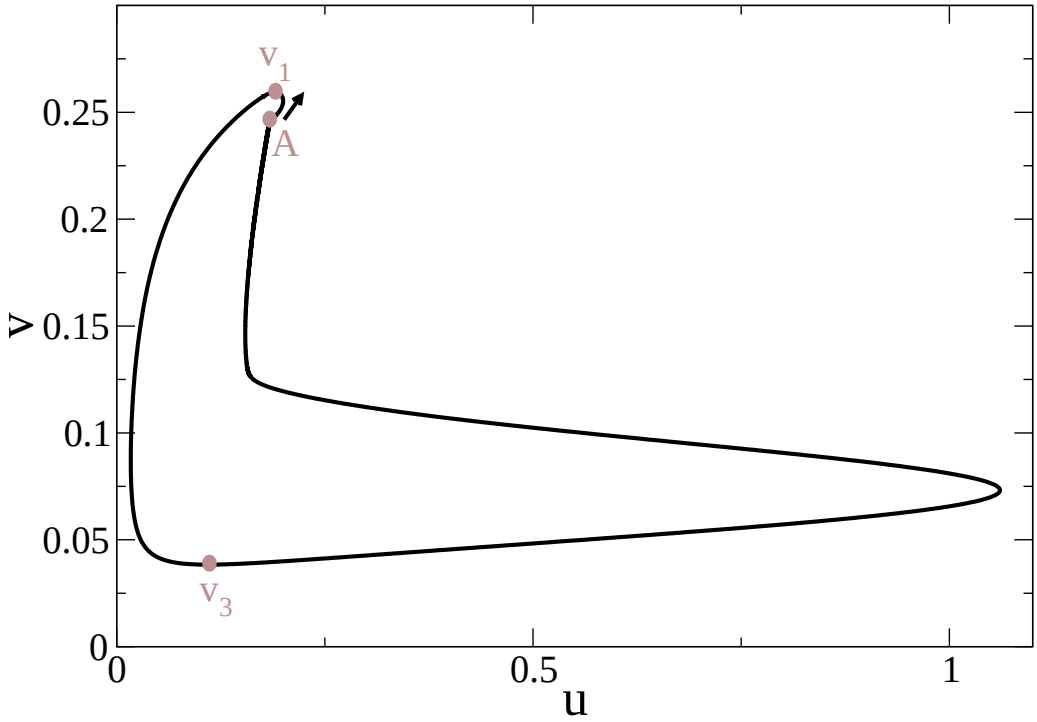

Figure 9. Homoclinic loop of system (12)-(14) with $k^\dagger = 0, k = 700$; the equilibrium (17) is denoted by A.

for $t > t_3$, see Fig. 9.

4. Conclusion

We have demonstrated the existence of robust families of homoclinic trajectories for operator-differential equations (1), (2) with the Preisach hysteresis operator. These systems can be considered as switching systems where switching from one planar ordinary differential equation to another occurs when a variable either passes a turning point or achieves a value stored in the memory state of the hysteresis operator. Homoclinic trajectories are possible when the basin of attraction of an equilibrium of one planar system in forward time overlaps with the basin of attraction of the equilibrium of another planar system in reversed time.

Acknowledgements

A. P. acknowledges the support of SFB 787 of the DFG. D. R. acknowledges the support of NSF through grant DMS-1413223.

References

[1] Krasnosel'skii M A and Pokrovskii A V 1989 *Systems with Hysteresis* (Springer, New York) zbl 0665.47038, MR0987431
[2] Visintin A 1994 *Differential Models of Hysteresis* (Springer, Berlin) mR1329094
[3] Brokate M and Sprekels J 1996 *Hysteresis and Phase Transitions* (Berlin: Springer) zbl 0951.74002, MR1411908
[4] Krejčı P and Recupero V 2014 Bv solutions of rate independent differential inclusions *Mathematica Bohemica* **139** 607–619
[5] Krejčí P 1996 *Hysteresis, Convexity and Dissipation in Hyperbolic Equations* (Gakkotosho, Tokyo) zbl 1187.35003, MR2466538

[6] Mielke A, Rossi R and Savaré G 2012 Variational convergence of gradient flows and rate-independent evolutions in metric spaces *Milan J. Math.* **80** 381–410
[7] Brokate M, Pokrovskii A and Rachinskii D 2006 Asymptotic stability of continuum sets of periodic solutions to systems with hysteresis *Journal of Differential Equations* **319** 94–109 zbl 1111.34035, MR2217849, DOI 10.1016/j.jmaa.2006.02.060
[8] Rachinskii D 1999 Asymptotic stability of large-amplitude oscillations in systems with hysteresis *Nonlinear Differential Equations and Applications NoDEA* **6** 267–288
[9] Krasnosel'skii A and Rachinskii D 2002 On a bifurcation governed by hysteresis nonlinearity *Nonlinear Differential Equations and Applications (NoDEA)* **9** 93–115 zbl 1013.34036, MR1891697, DOI 10.1007/s00030-002-8120-2
[10] Krasnosel'skii A and Rachinskii D I 2001 On the continua of cycles in systems with hysteresis *DOKLADY MATHEMATICS C/C OF DOKLADY-AKADEMIIA NAUK* **63** 339–344 zbl 1052.34052, MR1863745
[11] Diamond P, Rachinskii D and Yumagulov M 2000 Stability of large cycles in a nonsmooth problem with Hopf bifurcation at infinity *Nonlinear Analysis: Theory, Methods & Applications* **42** 1017–1031 zbl 0963.34034, MR1780452, DOI 10.1016/S0362-546X(99)00162-5
[12] Krasnosel'skii A and Rachinskii D 2005 Bifurcation of forced periodic oscillations for equations with preisach hysteresis *Journal of Physics: Conference Series* **22** 93
[13] Brokate M, Pokrovskii A, Rachinskii D and Rasskazov O 2005 *The Science of Hysteresis* vol I ed Mayergoyz I and Bertotti G (Elsevier, Academic Press) chap II, pp 125–291 zbl 1142.34026, MR2307929
[14] Eleuteri M, Kopfova J and KrejčıP 2015 A new phase field model for material fatigue in an oscillating elastoplastic beam *Discret Cont. Dyn. S. A* **35** 2465–2495
[15] Ruderman M, Hoffmann F and Bertram T 2009 Modeling and identification of elastic robot joints with hysteresis and backlash *IEEE Tran. Ind. Electron* **56** 3840–3847
[16] Mayergoyz I 2003 *Mathematical Models of Hysteresis and Their Applications* (Elsevier) zbl 0723.73003, MR1083150
[17] Appelbe B, Rachinskii D and Zhezherun A 2008 Hopf bifurcation in a van der Pol type oscillator with magnetic hysteresis *Physica B: Condensed Matter* **403** 301–304 dOI 10.1016/j.physb.2007.08.034
[18] Kuhnen K 2003 Modeling, identification and compensation of complex hysteretic nonlinearities - a modified Prandtl-Ishlinskii approach *European Journal of Control* **9** 407–418 dOI 10.3166/ejc.9.407-418
[19] Davino D, Krejčí P and Visone C 2013 Fully coupled modeling of magneto-mechanical hysteresis through 'thermodynamic' compatibility *Smart Materials and Structures* **22** 095009 dOI 10.1088/0964-1726/22/9/095009 URL `http://stacks.iop.org/0964-1726/22/i=9/a=095009`
[20] Aström K J 1995 *Adaptive Control, Filtering and Signal Processing* ed Aström K J, Goodwin G C and Kumar P R (Springer) pp 381–410
[21] Dimial M and Andrei P 2014 *'Noise-Driven Phenomena in Hysteretic Systems* (Springer) zbl 0723.73003, MR1083150
[22] Gurevich P L, Jaeger W and Skubachevskii A L 2009 On periodicity of solutions for thermocontrol problems with hysteresis-type switches *SIAM J. Math. Anal.* **41** 733–752
[23] KrejčıP, Rocca E and Sprekels J 2007 Non-local temperature-dependent phase-field models for non-isothermal phase transitions *Journal London Mathematical Society* **76** 197–210
[24] Appelbe B, Flynn D, McNamara H, O'Kane P, Pimenov A, Pokrovskii A, Rachinskii D and Zhezherun A 2009 Rate-independent hysteresis in terrestrial hydrology *Control Systems Magazine, IEEE* **29** 44–69 dOI 10.1109/MCS.2008.930923
[25] Krejčí P, O'Kane J P, Pokrovskii A and Rachinskii D 2011 Stability results for a soil model with singular hysteretic hydrology *Journal of Physics: Conference Series* **268** 012016 dOI 10.1088/1742-6596/268/1/012016
[26] Pimenov A, Kelly T C, Korobeinikov A, O'Callaghan M J, Pokrovskii A V and Rachinskii D 2012 Memory effects in population dynamics: Spread of infectious disease as a case study *Mathematical Modelling of Natural Phenomena* **7** 204–226 zbl 06074655, MR2928740, DOI 10.1051/mmnp/20127313
[27] Chiu C, Hoppensteadt F C and Jäger W 1994 Analysis and computer simulation of accretion patterns in bacterial cultures *J. Math. Biol.* **32** 841–855
[28] Friedman G, McCarthy S and Rachinskii D 2014 Hysteresis can grant fitness in stochastically varying environment *PLOS ONE* **9** e103241
[29] Cross R, Grinfeld M, Lamba H and Seaman T 2005 A threshold model of investor psychology *Physica A: Statistical Mechanics and its Applications* **354** 463–478
[30] Cross R, McNamara H, Pokrovskii A and Rachinskii D 2008 A new paradigm for modelling hysteresis in macroeconomic flows *Physica B: Condensed Matter* **403** 231–236 dOI 10.1016/j.physb.2007.08.017
[31] KrejčıP, Lamba H, Melnik S and Rachinskii D 2014 Analytical solution for a class of network dynamics with mechanical and financial applications *Phys. Rev. E* **90** 032822

[32] Mayergoyz I and Bertotti G (eds) 2005 *The Science of Hysteresis, 3-volume set* (Elsevier, Academic Press) zbl 1142.34028, MR2307931
[33] Pimenov A and Rachinskii D 2009 Linear stability analysis of systems with Preisach memory *Discrete and Continuous Dynamical Systems - Series B* **11** 997–1018 zbl 1181.47075, MR2505656, DOI 10.3934/dcdsb.2009.11.997
[34] Pokrovskii A, Power T, Rachinskii D and Zhezherun A 2006 Differentiability of evolution operators for dynamical systems with hysteresis *Journal of Physics: Conference Series* **55** 171 dOI 10.1088/1742-6596/55/1/017
[35] Krejčí P, O'Kane J P, Pokrovskii A and Rachinskii D 2012 Properties of solutions to a class of differential models incorporating Preisach hysteresis operator *Physica D: Nonlinear Phenomena* **241** 2010–2028 mR2994340, DOI 10.1016/j.physd.2011.05.005
[36] McCarthy S and Rachinskii D 2014 Dynamics of systems with Preisach memory near equilibria *Mathematica Bohemica* **139** 39–73
[37] Pimenov A and Rachinskii D 2014 Homoclinic orbits in a two-patch predator-prey model with preisach hysteresis operator *Mathematica Bohemica* **139** 285–298
[38] Pimenov A, Kelly T C, Korobeinikov A, O'Callaghan M J A and Rachinskii D 2015 Adaptive behaviour and multiple equilibrium states in a predator-prey model *Theoretical Population Biology* **101** 24–30